Semiconductor Physics, Quantum Electronics & Optoelectronics, 2024. V. 27, No 3. P. 337-347.

Optoelectronics and optoelectronic devices

Increasing the efficiency of CIGS solar cells due to the reduced graphene oxide field layer of the back surface

D. Fatihi[1], M.P. Bhandari[2], S. Golovynskyi[3], K. Abderrafi[1], R. Adhiri[1]

[1]*Laboratory of Engineering and Materials (LIMAT), Faculty of Sciences Ben M'sik, Hassan II University of Casablanca, Morocco*
[2]*Institute of Clinical and Preventive Medicine, University of Latvia, LV-1586 Riga, Latvia*
[3]*College of Physics and Optoelectronic Engineering, Shenzhen University, 518060, Shenzhen, P.R. China*
[*]*Correspondence author e-mail: fatihidounia31@gmail.com*

Abstract. Copper indium gallium selenide solar cells (CIGS-SCs) have gained attention due to their cost-effectiveness and environmentally friendly characteristics, making them a promising option for future electricity generation. The efficiency of CIGS-SCs can be enhanced by adding a back surface field layer (BSFL) under the absorber layer to reduce recombination losses. In this study, the electrical parameters, such as the series resistance, shunt resistance, and ideality factor, are calculated for CIGS-SCs with an advanced design, using the SC capacitance simulator (SCAPS) software. The detailed model used in the simulations considers the material properties and fabrication process of BSFL. By utilizing a reduced graphene oxide (rGO) BSFL, a conversion efficiency of 24% and a significant increase in the fill factor are predicted. This increase is primarily attributed to the ability of the rGO layer to mitigate the recombination of charge carriers and establish a quasi-ohmic contact at the metal-semiconductor interface. At higher temperatures, BSFL can become less effective due to an increased recombination and, in turn, a decreased carrier lifetime. Overall, this study provides valuable insights into the underlying physics of CIGS-SCs with BSFL and highlights the potential for improving their efficiency through advanced design and fabrication techniques.

Keywords: CIGS, solar cells, reduced graphene oxide (rGO), back surface layer, SCAPS.

https://doi.org/10.15407/spqeo27.03.337
PACS 68.65.Pq, 88.40.H-

Manuscript received 04.04.24; revised version received 12.07.24; accepted for publication 11.09.24; published online 20.09.24.

1. Introduction

Solar cells (SCs) are a critical technology for creating a cleaner and more sustainable future. SC development offers renewable energy generation, energy independence through reduced reliance on fossil fuels and oil imports as well as cost-effectiveness through affordable energy generation. SCs have gained significant importance in recent years and will continue to expand in significance as we strive for a more sustainable future.

Copper indium gallium selenide (CuInGaSe, CIGS) SCs are a type of thin-film SC technology that offers high efficiency, low cost, flexibility, good low-light performance, and durability [1–3]. These properties make CIGS-SCs well suited for various applications, such as building-integrated photovoltaic, portable electronic devices, spacecraft, and their stability to high-power radiation [4]. Thin-film SCs are a type of SC made using a thin layer of absorber material. These SCs are lightweight, flexible, and can be produced using low-cost and high-throughput processes. There are several types of thin-film SCs based on cadmium telluride (CdTe) [5], CIGS [6, 7], Cu_2ZnSnS_4 [8], silicon [9, 10], organic photovoltaic [11], perovskite [12, 13] and tin selenide (SnSe) [14]. Each of these SC types has unique properties and advantages that make them useful in different applications.

CIGS-SCs are known for their high efficiency and flexibility, while perovskite SCs have only the potential to be stable, low-cost, and highly-efficient. Although thin-film SCs are still less commonly used than traditional silicon-based SCs, they offer great promise for the future of solar energy due to their low cost, flexibility, and versatility. In and Ga are rare and expensive elements used in CIGS-SCs that can increase the cost of their production and lead to supply

competition [15]. Their use can also affect the electrical properties of SCs, with excessive In reducing efficiency and In substituting by Ga in the upper layers also potentially affecting properties. In and Ga are toxic elements, leading to safety and health concerns. Hence, manufacturers are seeking more sustainable and environmentally friendly alternatives to reduce the use of these elements and produce more efficient and cost-effective SCs.

Molybdenum (Mo) is used as a back contact. During the deposition of CIGS for SCs, the presence of Mo can cause a reaction with Se resulting in formation of molybdenum diselenide ($MoSe_2$). If the interface between Mo and CIGS is free of $MoSe_2$, a Schottky diode is formed, which acts as a barrier to the flow of carriers and leads to resistive losses in SC [16]. However, when Mo reacts with Se, the structure becomes CIGS/$MoSe_2$/Mo. $MoSe_2$ is a semiconductor with a bandgap (E_g) equal to 1.41 eV [17], and this configuration gives an ohmic behavior to the CIGS/Mo heterocontact. Therefore, to establish the ohmic contact with the CIGS absorber layer, it is necessary to use a metal with a low work function. However, this can be challenging due to the high barrier height between metal and CIGS. One effective solution is incorporating an extra layer formed from the back surface field layer (BSFL) material. This additional layer reduces the barrier height or narrows its width, thereby facilitating the formation of the ohmic contact.

This theoretical research aims to predict how to improve the overall effectiveness of the SC concept by fine-tuning the parameters of the CIGS and BSF layers [18]. This research uses the one-dimension solar cell capacitance simulator (SCAPS) software, which supports simulations based on the Poisson equation and carrier transport principles. The critical parameters, namely: steady-state energy band diagram, interface recombination, and carrier transport, can be calculated and analyzed using these simulations. The ultimate aim of this research is to increase the SC efficiency using a comprehensive evaluation of factors like quantum efficiency, electron affinity, E_g, and device temperature, T. The overarching goal is to optimize the SC parameters for significantly improved overall performance for advanced renewable energy generation.

2. Materials and methods

2.1. Simulation of the proposed configuration

SCAPS is a widely used software tool for simulating and analyzing semiconductor device behavior by numerically solving fundamental equations in semiconductor physics, including the Poisson equation, continuity equation, and drift-diffusion equation [19]. These equations describe the fundamental physics of semiconductor materials and devices, including the behavior of charge carriers, *i.e.* electrons (n) and holes (p), under the influence of electric fields and temperature (T). These equations can be written as follows.

The Poisson equation describes the electric potential in a semiconductor device and is given as

$$\frac{d^2\psi(x)}{dx^2} = \frac{e}{\varepsilon_0 \varepsilon_r}(x) - n(x) + N_D - N_A + \rho_p - \rho_n , \qquad (1)$$

where ψ is the electrostatic potential, ρ is the charge density, N_A and N_D are the acceptor and donor densities, e is the elementary charge, ε_0 is the vacuum permittivity, $\varepsilon_r(x)$ is the relative permittivity (dielectric constant), and $n(x)$ is the carrier concentration.

The continuity equations for electrons and holes are given as [20]

$$-\frac{1}{q}\frac{J_n}{d_x} = G - R \qquad (2)$$

and

$$-\frac{1}{q}\frac{J_p}{d_x} = G - R , \qquad (3)$$

respectively. J_n and J_p are the electron and hole current densities, respectively, q is the elementary charge, G is the generation rate of electron-hole (e-h) pairs, and R is the recombination rate of e-h pairs.

The current density for electrons and holes can be expressed as

$$J_n = D_n \frac{dn}{dx} + \mu_n n \frac{d\varphi}{dx} , \qquad (4)$$

$$J_p = D_p \frac{dp}{dx} + \mu_p p \frac{d\varphi}{dx} , \qquad (5)$$

where μ_n and μ_p are the electron and hole mobilities, D_n and D_p are the electron and hole diffusion coefficients, and φ is the electrostatic potential. SCAPS supports the numerical methods for predicting the semiconductor device behavior, using material properties, geometry, and boundary conditions as input data, and outputs electrical characteristics like I–V and C–V curves.

Fig. 1 shows a CIGS-SC structure composed of several layers arranged in the following order: an aluminum-doped zinc oxide (ZnO:Al) layer, an intrinsic zinc oxide (i-ZnO) layer, a cadmium sulfide (CdS) layer, a p-type CIGS absorber layer, a reduced graphene oxide (rGO) BSFL, and a Mo layer placed at the bottom.

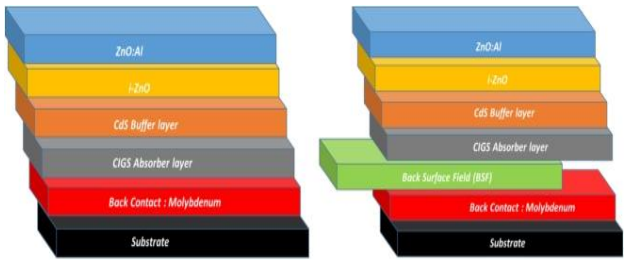

(a) (b)

Fig. 1. The designs of a conventional CIGS solar cell (a) adopted from [18, 21, 25] and a proposed cell with BSFL (b).

Table 1. Parameters of simulation used in the layers of solar cells.

Parameters	Layer material				
	CIGS [26]	CdS [27]	ZnO [28]	Al:ZnO [29]	rGO [21, 30, 31]
Thickness (μm)	3	0.05	0.6	1	0.03…0.1
Bandgap (eV)	1.3	2.4	3.4	3.4	1.09
Electron affinity (eV)	4.5	4.4	4.6	4.6	3.2
Dielectric permittivity (m^{-1})	13.6	10	9	9	10
CB density of states (m^{-3})	$2.2\cdot10^{18}$	$2.2\cdot10^{18}$	$2.2\cdot10^{18}$	$2.2\cdot10^{18}$	$2.2\cdot10^{18}$
VB density of states (m^{-3})	$1.8\cdot10^{19}$	$1.8\cdot10^{19}$	$1.8\cdot10^{19}$	–	$2\cdot10^{18}$
Electron/hole mobility ($cm^2V^{-1}S^{-1}$)	100/25	100/25	100/25	100/25	320/123
Electron thermal velocity (cm/s)	10^7	10^7	10^7	10^7	–
Hole thermal velocity (cm/s)	10^7	10^7	10^7	10^7	–
Defect density (cm^{-3})	10^{14}	10^{15}	10^{15}	10^{15}	10^{15}
Acceptor density (cm^{-3})	$1.1\cdot10^{18}$	–	–	–	$2\cdot10^{18}$

The function of the rGO layer is to enhance the SC performance by acting as BSFL between the absorber and the back Mo contact. This structure is being compared to a conventional CIGS-SC without BSFL. E_g of rGO varies depending on the synthesis method and the degree of reduction. Generally, GO has a much higher E_g than graphene due to oxygen-containing functional groups disrupting the graphene lattice conjugation. The reduction of GO removes some of these functional groups and restores the conjugation, leading to a decrease in E_g. GO has E_g of ~ 2.2 eV, while rGO exhibits E_g within the range 1.00…1.69 eV [21–23], depending on the degree of reduction. We used E_g = 1.09 eV for rGO [24].

2.2. Material parameter

Numerical simulations, particularly using the SCAPS program, have played a crucial role in advancing our understanding of chalcogenide-based SCs. SCAPS relies on fundamental semiconductor physics equations, including continuity equations for free electrons and holes, as well as the Poisson equation. It offers extensive parameter customization, namely: bandgap, electron affinity, mobility, doping, *etc*. Various lighting spectra are available, including AM0, AM1.5D, monochromatic, and more, alongside standard test conditions (STC) like global air mass (AM 1.5G), 300 K, and 1000 W/m^2 incident light power. Table 1 shows the characteristics of layers used for the simulated SCs.

3. Results

SCAPS was used to study how the photoelectrical properties of CIGS-SCs can be influenced by reducing the thickness of the absorber layer. The numerical outcomes also demonstrate the impact of the incorporated rGO as BSFL on the device performance. This work investigated the effects of adjusting the thickness of the CIGS and BSF layers, as well as *T*, on the photovoltaic properties of SC.

3.1. Conventional CIGS solar cell

3.1.1. Thickness adjusting of the CIGS absorber layer

This section aims to analyze the performance of ZnO/CdS/CIGS-SCs with different CIGS absorber layer thicknesses using the parameters presented in Table 1. The primary objective is to determine the optimal absorber layer thickness for SC.

Fig. 2 presents the trends of fill factor (FF), open-circuit voltage (V_{OC}), short-circuit current density (J_{SC}), and efficiency (η) for SC as a function of the *p*-CIGS absorber layer thickness within the range 0.5…3 μm. One can see that the thickness of the absorber layer has a considerable impact on all parameters. They increase significantly with the absorber layer thickness. Particularly, J_{SC} increased from 27.1 to 33.3 mA/cm^2. This is mainly caused by the back surface recombination that occurs at the interface between CIGS and Mo. Due to the reduced thickness of the layer, high-energy photons (short wavelengths) can penetrate deeply into the layer and generate e-h pairs in the CIGS/Mo contact area. However, most of these e-h pairs recombine in this region, which results in a lower J_{SC}. Furthermore, when the layer thickness is further reduced to 0.5 μm, degradation of V_{OC} drops to 0.75 V. The fluctuation in V_{OC} is caused by recombination of photogenerated carriers.

As a result of the decrease in V_{OC} and J_{SC}, the device efficiency decreases. According to a recent investigation, the CIGS-SCs exhibit the highest efficiency at a thickness of 3 μm [32]. At this thickness, we calculated V_{OC} = 0.81 V, J_{SC} = 34.48 mA/cm^2 and FF = 83.35%, resulting in η = 23.33%. These values were compared with the reference values, and it was found that FF was similar to the reference value of 83% [18]. V_{OC} is within the range 0.81…0.82 V [33, 34], while J_{SC} = 34.13 mA/cm^2 [35]. It is worth noting that reducing the absorber thickness can result in the back contact being too close to the depletion band [36, 37], leading to similar changes in the performance parameters as reported in other studies [38].

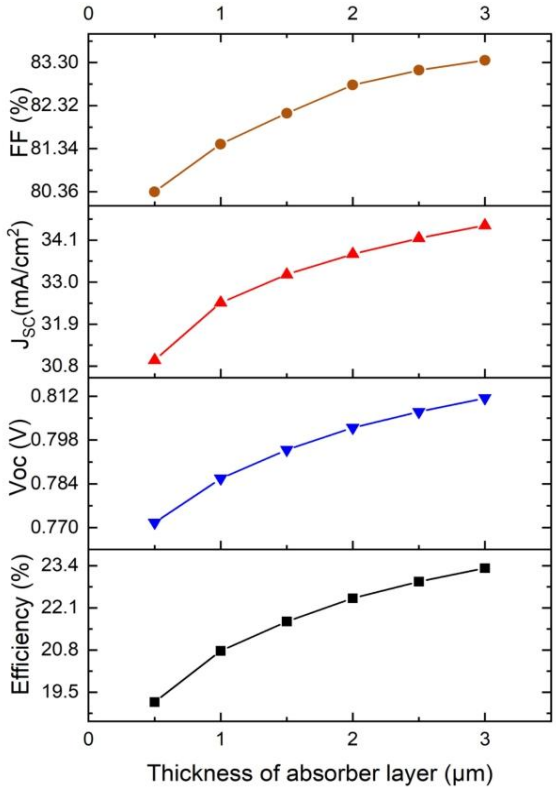

Fig. 2. Photovoltaic performances of the CIGS solar cells as a function of the absorber thickness: FF (fill factor), V_{OC} (open-circuit voltage), J_{SC} (short-circuit current), and efficiency.

3.1.2. Quantum efficiency of the CIGS layer at different thicknesses

Figs. 3 shows the quantum efficiency (QE) spectrum of the studied SC of different CIGS thicknesses, where QE increases with the thickness. This occurs because thicker layers will increase the number of photons, as well as the production and collection of e-h pairs. Initially, for the thin layer measuring just 0.5 μm, QE exhibits a gradual decline after the absorption peak, approximately at 500 nm (Fig. 3). As the thickness exceeds 2.5 μm, minimal discernible shifts in QE are observed. This implies that the electrical parameters demonstrate a notable elevation up to this threshold layer thickness.

3.2. CIGS solar cell with rGO BSFL

3.2.1. Comparison of conventional and proposed solar cell with rGO BSFL

Being based on previously mentioned findings, we can summarize that the SC with a thickness of 3 μm is ideal. After embedding BSFL with the thickness 0.03 μm, we detect an increase in the SC efficiency up to 24.54%. Fig. 4 shows the behavior of fill factor, open-circuit voltage, short-circuit current density, and efficiency for SCs with BSFL layer and without it as a function of the *p*-CIGS absorber layer thickness within the range 0.5…3 μm, while the rGO thickness is 0.03 μm. As we can see, under the same absorption layer thickness, the proposed cell significantly improved all photovoltaic

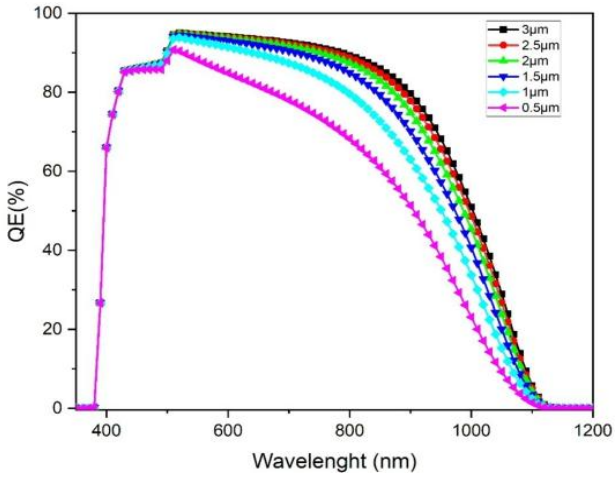

Fig. 3. Quantum efficiency spectra of the CIGS absorber layer of different thicknesses. (Color online)

performances. The efficiency of the conventional CIGS-SC with a 1.5-μm absorber layer is 21.67%. However, when a thin 0.03-μm rGO BSFL is embedded, the efficiency of modified CIGS/rGO-SC increases to 23.44%. This finding is in line with the theoretical study reported in the literature [39–41] along with one experimental study [42]. The mentioned increase can be explained by the following. Both rGO and CIGS operate as absorbers (with a total thickness of 1.53 μm), with rGO assisting in increasing the photon energy absorption by the cell. Fig. 5, which displays the band diagram of these two SCs produced using SCAPS, explains this. The extra layer of rGO, by which a quasi-ohmic contact is generated at the metal (Mo) – semiconductor (CIGS) interface, can be the reason of the improvement in the photovoltaic parameters: it reduces recombination at the rear surface, increases V_{OC} and J_{SC}. As a result, a huge number of photons can be collected and more e-h pairs are generated. Changing the standard cell design to the one with the rGO BSFL described herein, J_{SC} rises from 33.2 to 34.39 mA/cm^2, and V_{OC} increases from 0.79 to 0.82 V. Therefore, 1.5 μm is the ideal absorber layer thickness for the proposed cell. The decrease in the CIGS layer thickness will certainly reduce the cost of SC fabrication.

3.2.2. Adjusting of the BSFL thickness

To enhance the SC efficiency, the thickness of the rGO layer was varied within the range of 0.03…0.1 μm, while the thickness of the CIGS layer was constant (1.5 μm) as depicted in Fig. 6.

The experimental results indicated a significant increase in the efficiency from 0.03% to 23.44%, which further improved to 23.94% for a thickness of 0.05 μm in the rGO layer. However, beyond this thickness, the figures show no substantial change in the efficiency. Nevertheless, some experimental findings reveal that a thicker layer might not be suitable as it could result in increased series resistance, leading to a reduced overall SC efficiency. Consequently, FF decreases with a thicker BSFL.

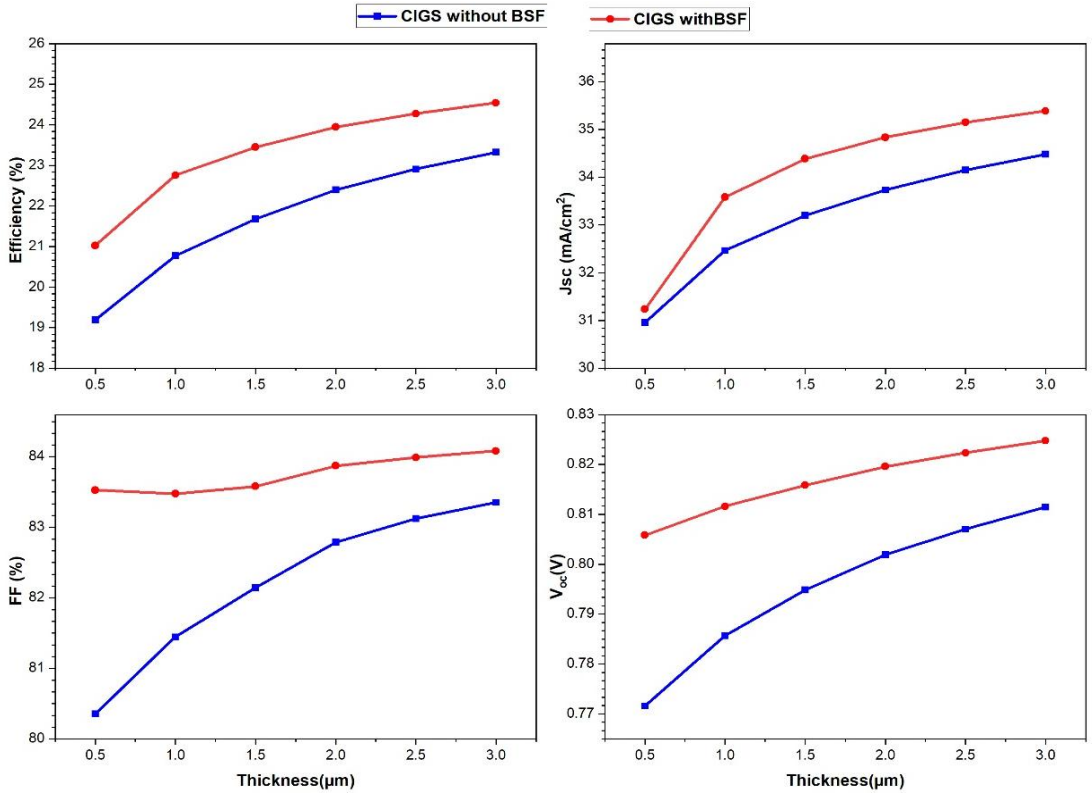

Fig. 4. Photovoltaic performances of the studied CIGS solar cells with (red circles) and without (blue squares) rGO BSFL.(Color online)

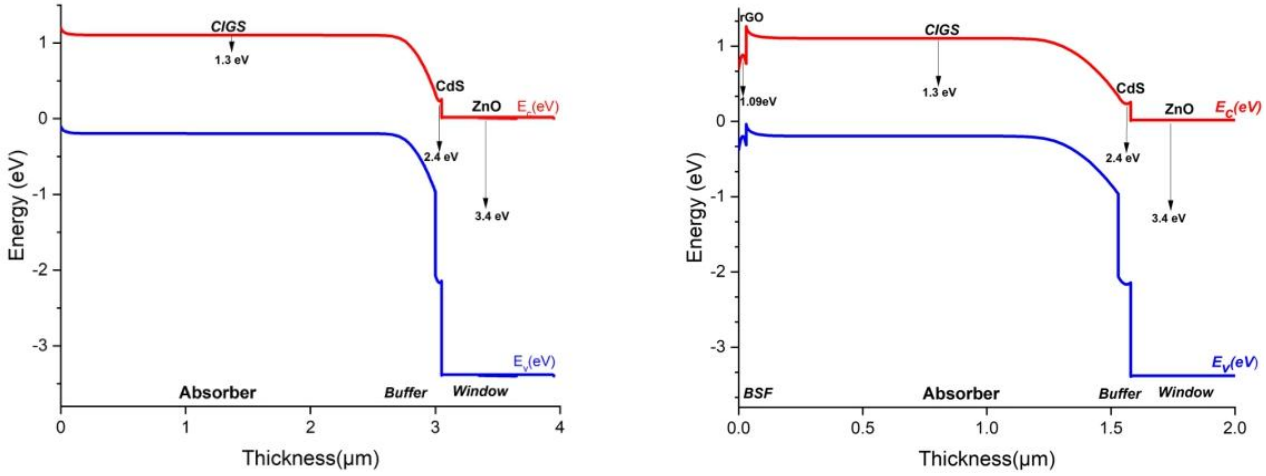

Fig. 5. The SCAPS created an energy band diagram without (left) and with rGO BSFL (right). (Color online)

3.2.3. The impact on quantum efficiency

Fig. 7 displays the simulated QE spectra for these two device structures. Due to improved photon absorption by the thicker absorber layers, the QE of CIGS/rGO-SCs initially increases with increasing the CIGS layer thickness. BSFL serves as a reflector and is critical in boosting light-collection performance. Photon absorption is reduced as back reflectivity improves, boosting QE. After adding BSFL, the QE is enhanced to a high level of 95.44% at 500 nm due to an increased collection of photons at longer wavelengths within the range of 500 to 1000 nm. Due to the device producing more e-h pairs as a result of high absorption, the current density rises. Additionally, because each substance can only absorb photons within a specific wavelength range of the visible light spectrum, all curves begin to fall toward a zero QE around 1000…1100 nm.

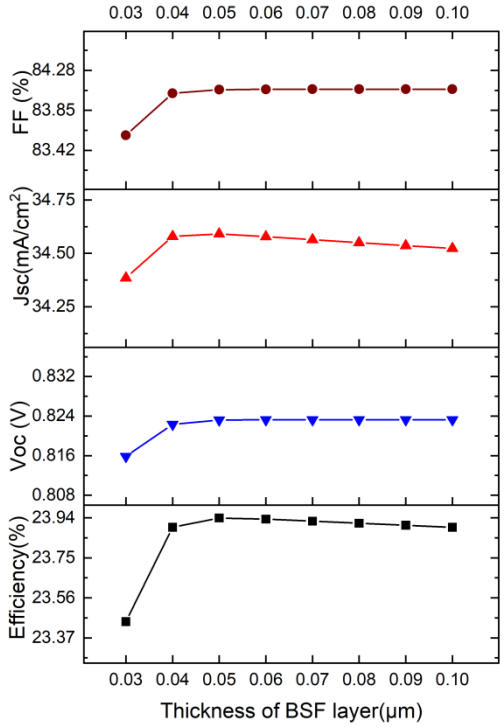

Fig. 6. Photovoltaic characteristics of CIGS solar cells at the different rGO thickness: fill factor, J_{SC}, V_{OC} and efficiency.

Recycling is necessary to guarantee a future supply of both elements (In and Ga) used in CIGS and keep manufacturing costs low [43]. Compared with other thin-film SCs, In and Ga are the most effective materials. Unfortunately, they are costly components in CIGS-SCs [44, 45], so it is not advisable to produce absorbers with thicker CIGS layers. Similarly, reducing the thickness of the CIGS material can lower the quantities of Ga and In required, therefore, lowering SC production cost. In addition, these results show an improved efficiency when using the new cost-effective SC layout as compared to old designs, since rGO is less expensive and more generally accessible than Ga and In. Thus, our findings can help to produce CIGS-SCs at a higher profit.

3.2.4. Effect of operating temperature on CIGS solar cell

T influences the performance of CIGS-SCs. As T rises, V_{OC} and FF of the cell typically decrease, while J_{SC} rises in Fig. 8. We varied T from 290 to 390 K. At high T, this reduces the cell overall power output. The Shockley–Queisser theory can model the temperature dependence of the photovoltaic parameters of CIGS-SCs. The relationship between J_{SC} and V_{OC} as a function of T is [46]

$$V_{OC} = \frac{nkT}{q} \log\left(\frac{J_{SC}}{J_0}\right), \quad (6)$$

where n is the ideality factor, k is the Boltzmann constant, q is the electron charge, and J_0 denotes the reverse saturation current.

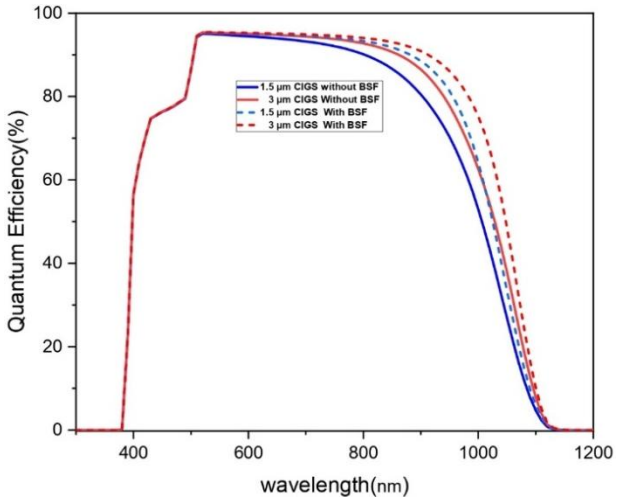

Fig. 7. Quantum efficiency spectra of the CIGS solar cells with and without rGO BSFL. (Color online)

The optimal operating T for CIGS-SCs is typically within 25…35 °C. It is worth noting that the temperature coefficient of CIGS is usually negative, meaning that SC efficiency decreases with T. For the initial CIGS-SCs, operating T can affect V_{OC}, J_{SC}, and FF (Fig. 9). At low T, V_{OC} increases due to reduced recombination rates, while J_{SC} drops due to decreased carrier mobility. As T rises, V_{OC} decreases due to increased intrinsic carrier concentration and reduced E_g, while J_{SC} increases due to amplified carrier mobility. However, FF decreases with T due to enlarged series resistance. It can be observed that CIGS/rGO-SCs generally have a higher performance than those without BSFL. In CIGS/rGO-SCs, operating T can affect the performance differently. Thin BSFL is deposited on the back surface of SC to reduce the recombination of charge carriers. At higher T, BSFL can become less effective due to a decrease in the carrier life-time.

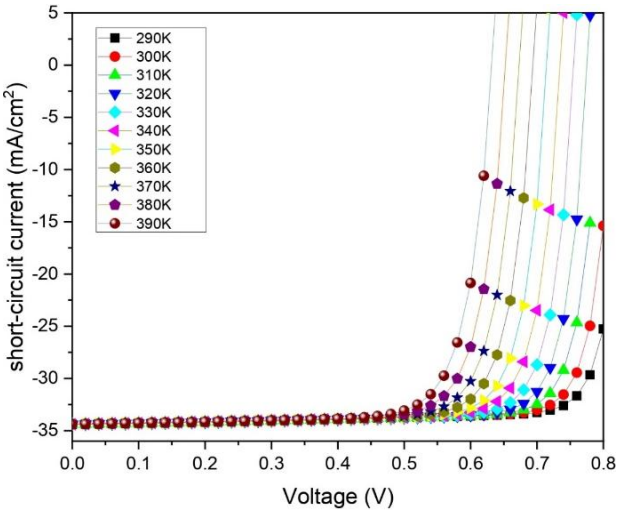

Fig. 8. Temperature-dependent *I–V* characteristics of a CIGS solar cell with rGO BSFL. (Color online)

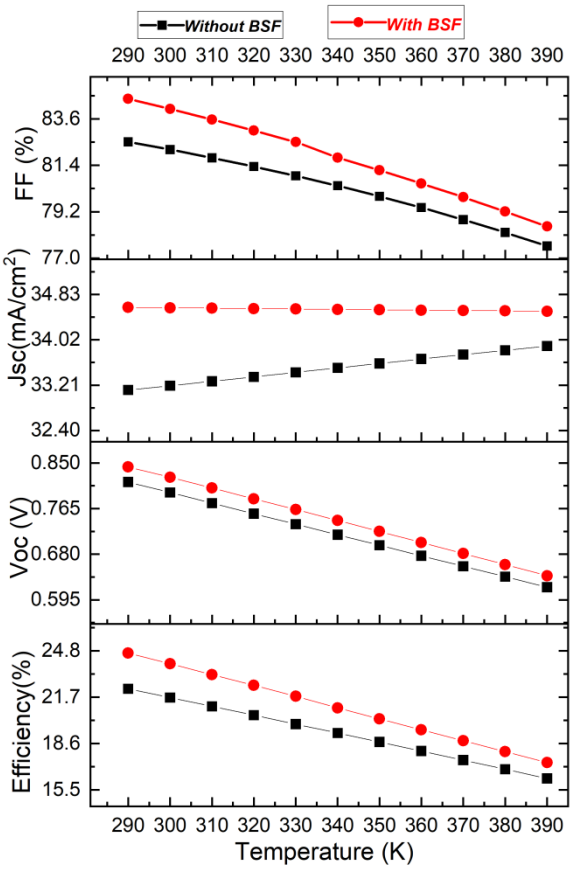

Fig. 9. Temperature dependences of photovoltaic characteristics of CIGS solar cells with and without rGO BSFL. (Color online)

Overall, the effect of operating *T* on CIGS-SCs depends on various factors, namely: the material properties, SC design, and operating conditions. However, it is important to keep the operating *T* of CIGS-SC within a certain range to ensure an optimal performance.

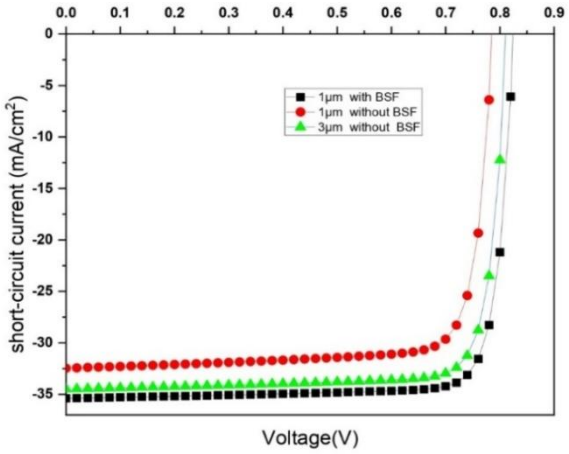

Fig. 10. *I–V* characteristics of CIGS solar cells with and without rGO BSFL. (Color online)

3.2.5. *I–V* characteristics of CIGS solar cells

The *I–V* characteristic of CIGS-SCs describes their performance under different electrical loads. Fig. 10 depicts the *I–V* curves at the optimal device settings with and without BSFL with absorber layers of various thicknesses. One can see that the CIGS/rGO-SC exhibits superior *I–V* characteristics as compared to that without BSFL, given that the CIGS thickness is 1.5 μm and the BSFL thickness is 0.05 μm.

Table 2 presents a summary of the photovoltaic performance of different SCs, including both experimental and simulation data. The data highlights the diverse range of experimental and simulated SCs, each exhibiting various performance. The efficiency of these SCs depends on the utilized materials and the presence or absence of BSFL. Additionally, the table underscores the importance of material selection and BSFL incorporation in achieving the enhanced photovoltaic performances.

Table 2. Enhanced photovoltaic performances of the proposed CIGS solar cell and those reported elsewhere.

Type of research	Absorber	BSF layer	Efficiency (%) without BSF	Efficiency (%) with BSF	References
Experimental	CIGS	–	19.90	–	[47]
Experimental	CIGS	–	18.10	–	[48]
Experimental	CdTe	Graphene	–	3.20	[40]
Simulation	ZnTe	Sb_2Te_3	7.14	18.33	[49]
Simulation	Cu_2ZnSnS_4	Cu_2ZnSnS_4	12.05	14.11	[50]
Simulation	CIGS	Si	16.39	21.33	[26]
Simulation	CIGS	–	22.67	–	[51]
Simulation	CZTSSe	SnS	12.30	15.70	[52]
Simulation	CdTe	Graphene	–	15.00	[40]
Simulation	CIGS	p^+ CIGS	20.78	21.95	[39]
Simulation	CIGS	rGO	21.68	23.94	this work

4. Conclusions

A CIGS solar cell with rGO BSFL was theoretically modeled and its electrical parameters were calculated. The BSFL plays a pivotal role in enhancing the efficiency of CIGS-SCs. Precisely tuning the composition, thickness, and fabricating BSFL is essential for achieving optimal performance. Ongoing research in this domain promises further advancements in CIGS-SCs and thin-film photovoltaics in general. We predicted an SC efficiency of 23.9% with rGO BSFL. This achievement prompted a comparative analysis between conventional SCs and those augmented with rGO BSFL. The results revealed a substantial enhancement in the efficiency, primarily attributed to the ability of the rGO layer to mitigate the back surface recombination and establish a quasi-ohmic contact at the metal-semiconductor interface. The combined thickness of the CIGS and rGO layers in this high-efficiency configuration was 1.5 and 0.05 μm, respectively, resulting in an overall efficiency of 23.9%.

The modeled structure, as shown in this research, holds a good potential as a viable option for thin-film SCs. Its success not only underscores the significance of BSFLs but also highlights the importance of innovative materials in pushing the boundaries of SC efficiency. This opens new options for renewable energy technologies, offering a promising path toward more efficient and sustainable photovoltaic solutions.

Conflicts of Interest

The authors declare no conflict of interest.

Acknowledgments

The authors would like thank to Dr. Marc Burgelman and his team at the Department of Electronics and Information Systems (ELIS), University of Gent, Belgium for providing the SCAPS software package, version 3.3.07. The authors would like to express their gratitude to the Ministry of Foreign Affairs and International Cooperation (MAECI) for their invaluable support in funding and facilitating this project. Dr. S. Golovynskyi acknowledges Key Research and Development Project of Guangdong Province (2020B010169003) for a partial support.

References

1. Sreevalsan A., Akash S., Pasha A. *et al.* Review on perovskite silicon tandem solar cells: Status and prospects 2T, 3T and 4T for real world conditions. *Mater. Des.* 2021. **211**. P. 110138. https://doi.org/10.1016/j.matdes.2021.110138.
2. Ghamsari-Yazdel F., Fattah A. Performance enhancement of CIGS solar cells using ITO as buffer layer. *Micro Nanostructures.* 2022. **168**. P. 207289. https://doi.org/10.1016/j.micrna.2022.207289.
3. Sivaraj S., Rathansamy R., Kaliyannan G. *et al.* A comprehensive review on current performance, challenges and progress in thin-film solar cells. *Energies.* 2022. **15**. P. 8688. https://doi.org/10.3390/en15228688.
4. Sharbati S., Gharibshahian I., Orouji A.A. Designing of $Al_xGa_{1-x}As$/CIGS tandem solar cell by analytical model. *Solar Energy.* 2019. **188**. P. 1–9. https://doi.org/10.1016/j.solener.2019.05.074.
5. Jain S.K., Sharma G., Vyas S. Influence of hole interface layer on the performance of cadmium telluride-based thin film solar cell. *Mater. Today: Proc.* 2023. **74**. P. 231–233. https://doi.org/10.1016/j.matpr.2022.08.058.
6. Boukortt N.E.I., Patanè S., Adouane M. Modeling and investigation of rear-passivated ultrathin CIGS solar cell. *Electronics.* 2023. **12**. P. 758. https://doi.org/10.3390/electronics12030758.
7. Violas A., Oliveira A.J., Teixeira J. *et al.* Will ultra-thin CIGS solar cells overtake the champion thin-film cells? Updated SCAPS baseline models reveal main differences between ultrathin and standard CIGS. *Sol. Energy Mater Sol. Cells.* 2022. **243**. P. 111792. https://doi.org/10.1016/j.solmat.2022.111792.
8. Babichuk I.S., Semenenko M.O., Golovynskyi S. *et al.* Control of secondary phases and disorder degree in Cu_2ZnSnS_4 films by sulfurization at varied subatmospheric pressures. *Sol. Energy Mater Sol. Cells.* 2019. **200**. P. 109915. https://doi.org/10.1016/j.solmat.2019.109915.
9. Yamamoto K., Nakajima A., Yoshimi M. *et al.* A high efficiency thin film silicon solar cell and module. *Solar Energy.* 2004. **77**. P. 939–949. https://doi.org/10.1016/j.solener.2004.08.028.
10. Sachenko A.V., Kostylyov V.P., Evstigneev M. Space charge region recombination in highly efficient silicon solar cells. *SPQEO.* 2024. **27**. P. 010–027. https://doi.org/10.15407/spqeo27.01.010.
11. Cui Y., Yao H., Hong L. *et al.* Organic photovoltaic cell with 17% efficiency and superior process-ability. *Natl. Sci. Rev.* 2020. **7**. P. 1239–1246. https://doi.org/10.1093/nsr/nwz200.
12. Guo Z., Jena A.K., Kim G.M., Miyasaka T. The high open-circuit voltage of perovskite solar cells: a review. *Energy Environ. Sci.* 2022. **15**. P. 3171–3222. https://doi.org/10.1039/D2EE00663D.
13. Abdulmalik M.O., Danladi E. Influence of perovskite thickness on the performance of silver-doped $NaZnBr_3$ perovskite solar cells using SCAPS software. *SPQEO.* 2023. **26**. P. 321–331. https://doi.org/10.15407/spqeo26.03.321.
14. Yadav R.K., Pawar P.S., Nandi R. *et al.* A qualitative study of SnSe thin film solar cells using SCAPS 1D and comparison with experimental results: A pathway towards 22.69% efficiency. *Sol. Energy Mater. Sol. Cells.* 2022. **244**. P. 111835. https://doi.org/10.1016/j.solmat.2022.111835.
15. Mir S., Vaishampayan A., Dhawan N. A review on recycling of end-of-life light-emitting diodes for metal recovery. *JOM.* 2022. **74**. P. 599–611. https://doi.org/10.1007/s11837-021-05043-9.
16. Sun H., Li P., Xue Y. *et al.* Effect of $MoSe_2$ on the performance of CIGS solar cells. *Optoelectronics Lett.* 2019. **15**. P. 428–434. https://doi.org/10.1007/s11801-019-9027-z.

17. Pan Y., Li S., Ye M. *et al.* Interfacial properties of monolayer $MoSe_2$–metal contacts. *J. Phys. Chem. C*. 2016. **120**. P. 13063–13070. https://doi.org/10.1021/acs.jpcc.6b02696.
18. Mostefaoui M., Mazari H., Khelifi S. *et al.* Simulation of high efficiency CIGS solar cells with SCAPS-1D software. *Energy Procedia*. 2015. **74**. P. 736–744. https://doi.org/10.1016/j.egypro.2015.07.809.
19. Alzoubi T., Moustafa M. Simulation analysis of functional $MoSe_2$ layer for ultra-thin $Cu(In,Ga)Se_2$ solar cells architecture. *Mod. Phys. Lett. B*. 2020. **34**. P. 2050065. https://doi.org/10.1142/S0217984920500657.
20. Li C., Luo H., Gu H., Li H. BTO-coupled CIGS solar cells with high performances. *Materials*. 2022. **15**. P. 5883. https://doi.org/10.3390/ma15175883.
21. Abid, Sehrawat P., Islam S.S. *et al.* Reduced graphene oxide (rGO) based wideband optical sensor and the role of temperature, defect states and quantum efficiency. *Sci. Rep.* 2018. **8**. P. 3537. https://doi.org/10.1038/s41598-018-21686-2.
22. Chang H., Sun Z., Saito M. *et al.* Regulating infrared photoresponses in reduced graphene oxide phototransistors by defect and atomic structure control. *ACS Nano*. 2013. **7**. P. 6310–6320. https://doi.org/10.1021/nn4023679.
23. Mattson E., Johns J., Pande K. *et al.* Vibrational excitations and low-energy electronic structure of epoxide-decorated graphene. *J. Phys. Chem. Lett.* 2014. **5**. P. 212–219. https://doi.org/10.1021/jz4025386.
24. Jeong W.-L., Park S., Jho Y. *et al.* The role of the graphene oxide (GO) and reduced graphene oxide (RGO) intermediate layer in CZTSSe thin-film solar cells. *Materials*. 2022. **15**. P. 3419. https://doi.org/10.3390/ma15103419.
25. Osman Y., Fedawy M., Abaza M., Aly M. Solar cell performance enhancement with optimized CIGS absorber bandgap and buffer layer. *J. Phys. Conf. Ser*. 2020. **1447**. P. 012057. https://doi.org/10.1088/1742-6596/1447/1/012057.
26. Heriche H., Rouabah Z., Bouarissa N. New ultra thin CIGS structure solar cells using SCAPS simulation program. *Int. J. Hydrogen Energ.* 2017. **42**. P. 9524–9532. https://doi.org/10.1016/j.ijhydene.2017.02.099.
27. Huang C.-H., Chuang W.-J. Dependence of performance parameters of CdTe solar cells on semiconductor properties studied by using SCAPS-1D. *Vacuum*. 2015. **118**. P. 32–37. https://doi.org/10.1016/j.vacuum.2015.03.008.
28. Shafi M.A., Bouich A., Fradi K. *et al.* Effect of deposition cycles on the properties of ZnO thin films deposited by spin coating method for CZTS-based solar cells. *Optik*. 2022. **258**. P. 168854. https://doi.org/10.1016/j.ijleo.2022.168854.
29. Ziabari S.A.M., Ziabari A.A., Mousavi S.J. Efficiency enhancement of thin-film solar cell by implementation of double-absorber and BSF layers: the effect of thickness and carrier concentration. *J. Comput. Electron.* 2022. **21**. P. 675–683. https://doi.org/10.1007/s10825-022-01878-w.
30. Wang Y., Chen Y., Lacey S.D. *et al.* Reduced graphene oxide film with record-high conductivity and mobility. *Mater. Today* 2018. **21**. P. 186–192. https://doi.org/10.1016/j.mattod.2017.10.008.
31. Nowsherwan G.A., Hussain S.S., Khan M. *et al.* Role of graphene-oxide and reduced-graphene-oxide on the performance of lead-free double perovskite solar cell. *Z. Naturforsch. A*. 2022. **77**. P. 1083–1098. https://doi.org/10.1515/zna-2022-0147.
32. Chadel M., Chadel A., Benyoucef B., Aillerie M. Enhancement in efficiency of CIGS solar cell by using a *p*-Si BSF layer. *Energies* 2023. **16**. P. 2956. https://doi.org/10.3390/en16072956.
33. Barman B., Kalita P.K. Influence of back surface field layer on enhancing the efficiency of CIGS solar cell. *Solar Energy*. 2021. **216**. P. 329–337. https://doi.org/10.1016/j.solener.2021.01.032.
34. Sylla A., Touré S., Vilcot J.-P. Numerical modeling and simulation of CIGS-based solar cells with ZnS buffer layer. *Open Journal of Modelling and Simulation*. 2017. **05**. P. 218. https://doi.org/10.4236/ojmsi.2017.54016.
35. Robin M.S.R., Rasmi M.M.M., Sarker Md.S.Z., Rabbi Al Mamun A.S.M. Numerical modeling and analysis of ultra thin film $Cu(In, Ga)Se_2$ solar cell using SCAPS-1D. *2016 3rd Int. Conf. on Electrical Engineering and Information Communication Technology* (*ICEEICT*), 2016. P. 1–5. https://doi.org/10.1109/CEEICT.2016.7873169.
36. Chelvanathan P., Hossain M.I., Amin N. Performance analysis of copper–indium–gallium–diselenide (CIGS) solar cells with various buffer layers by SCAPS. *Curr. Appl. Phys.* 2010. **10**. P. S387–S391. https://doi.org/10.1016/j.cap.2010.02.018.
37. Rafik Z., Bouchama I., Djedoui L., Zaidi E. Improving the efficiency of CIGS solar cells by inserting a BSF μc-Si:H layer. 2022. https://doi.org/10.21203/rs.3.rs-1177456/v1.
38. Heriche H., Rouabah Z., Bouarissa N. High-efficiency CIGS solar cells with optimization of layers thickness and doping. *Optik*. 2016. **127**. P. 11751–11757. https://doi.org/10.1016/j.ijleo.2016.09.071.
39. Ehemba A.K., Socé M.M., Domingo J.J. *et al.* Optimization of the properties of the back surface field of a $Cu(In,Ga)Se_2$ thin film solar cell. *AJER*. 2017. **5**. P. 57–62. https://doi.org/10.12691/ajer-5-2-5.
40. Kc D., Shah D.K., Akhtar M.S. *et al.* Numerical investigation of graphene as a back surface field layer on the performance of cadmium telluride solar cell. *Molecules*. 2021. **26**. P. 3275. https://doi.org/10.3390/molecules26113275.
41. Kumari R., Mamta, Kumar R., Singh V.N. SnTe as a BSF enhances the performance of Sb_2Se_3 based solar cell: A numerical approach. *Heliyon*. 2022. **8**. P. e12043. https://doi.org/10.1016/j.heliyon.2022.e12043.
42. Green M.A., Dunlop E., Hohl-Ebinger J. *et al.* Solar cell efficiency tables (version 57). *Prog. Photovolt.: Res. Appl.* 2021. **29**, No 5. P. 3–15. https://doi.org/10.1002/pip. 3371.

43. Calvo G., Valero A. Strategic mineral resources: Availability and future estimations for the renewable energy sector. *Environ. Dev.* 2022. **41**. P. 100640. https://doi.org/10.1016/j.envdev.2021.100640.
44. Yunus N.A.Md, Aman N.H.N., Khoshsirat N. Comparison between thin-film solar cells and copper–indium–gallium–diselenide in Southeast Asia. *IET Renewable Power Generation*. 2015. **9**. P. 1079–1086. https://doi.org/10.1049/iet-rpg.2015.0114.
45. Pansuriya T., Malani R., Kheraj V. Investigations on the effect of buffer layer on CMTS based thin film solar cell using SCAPS 1-D. *Opt. Mater.* 2022. **126**. P. 112150. https://doi.org/10.1016/j.optmat.2022.112150.
46. Park Y., Lee S., Yi J. *et al.* Sputtered CdTe thin film solar cells with Cu_2Te/Au back contact. *Thin Solid Films.* 2013. **546**. P. 337–341. https://doi.org/10.1016/j.tsf.2013.02.108.
47. Repins I., Contreras M.A., Egaas B. *et al.* 19·9%-efficient ZnO/CdS/$CuInGaSe_2$ solar cell with 81·2% fill factor. *Prog. Photovolt.: Res. Appl.* 2008. **16**. P. 235–239. https://doi.org/10.1002/pip.822.
48. Nakada T., Mizutani M. 18% efficiency Cd-free Cu(In, Ga)Se_2 thin-film solar cells fabricated using chemical bath deposition (CBD)-ZnS buffer layers. *Jpn. J. Appl. Phys.* 2002. **41**. P. L165. https://doi.org/10.1143/JJAP.41.L165.
49. Sohid S.B., Kabalan A. Numerical analysis of ZnTe based solar cell with Sb_2Te_3 back surface field layer using SCAPS-1D. *2018 IEEE 7th World Conf. on Photovoltaic Energy Conversion* (*WCPEC*) (A Joint Conf. of 45th IEEE PVSC, 28th PVSEC & 34th EU PVSEC), 2018. P. 1852–1857. https://doi.org/10.1109/PVSC.2018.8547800.
50. Benzetta A.E.H., Abderrezek M., Djeghlal M.E. Contribution to improve the performances of Cu_2ZnSnS_4 thin-film solar cell via a back surface field layer. *Optik*. 2019. **181**. P. 220–230. https://doi.org/10.1016/j.ijleo.2018.12.048.
51. Lorbada R.V., Walter T., Marrón D.F. *et al.* A deep insight into the electronic properties of CIGS modules with monolithic interconnects based on 2D simulations with TCAD. *Coatings.* 2019. **9**. P. 128. https://doi.org/10.3390/coatings9020128.
52. Kumar A., Thakur A.D. Improvement of efficiency in CZTSSe solar cell by using back surface field. *IOP Conf. Ser.: Mater. Sci. Eng.* 2018. **360**. P. 012027. https://doi.org/10.1088/1757-899X/360/1/012027.

Authors' contributions

Fatihi D.: conceptualization, theoretical calculations, data curation, visualization, writing – original draft.
Bhandari M.P.: visualization, review and editing.
Golovynskyi S.: visualization, writing and editing.
Abderrafi K.: review, editing, visualization, supervision.
Adhiri R.: writing, review, funding acquisition, project administration, validation, supervision.

Authors and CV

Fatihi Dounia, acquired a Bachelor's degree in Physics in 2017 and a Master's degree in Renewable Energy and Energy Systems in 2019 from Hassan II University, Faculty of Science Ben M'Sik in Casablanca, Morocco. Currently, she is a PhD student at the same university, conducting continuous research in the energy field. Her main research area of interest is the application and improvement of solar energy-based systems. Additionally, she is currently under the MAECI scholarship in Italy. https://orcid.org/0000-0002-6949-0779

Manohar Prasad Bhandari obtained his Ph.D. from the University of Brescia, Italy in 2019. His PhD research focused on the application of an electronic nose prototype in food quality control. He then went to the Ben Gurion University of the Negev in Israel for a postdoctoral training. From 2020 until 2023, he was leading an EU-funded postdoctoral project at the University of Latvia, where he focused on the early detection of gastric cancer using metabolomics and breath analysis approaches. He is currently a postdoctoral associate at the Mechanical and Aerospace Engineering Department of the University of California, Davis, working somewhere between the realm of metabolomics and chemical sensors.
E-mail: manoharpbhandari@gmail.com,
https://orcid.org/0000-0003-2712-476X

Sergii Golovynskyi, defended his PhD thesis in Physics and Mathematics (Optics, Laser Physics) in 2012 at the Taras Shevchenko National University of Kyiv. In 2012, he started his research carrier in V. Lashkaryov Institute of Semiconductor Physics, NAS of Ukraine. Since 2016, he is an associate researcher at Shenzhen University, China. Author of more than 60 scientific articles, obtaining an H-index of 18. His main research activity is in the fields of semiconductor physics and optics, spectroscopy, nanomaterials and optoelectronics.
E-mail: serge@szu.edu.cn,
https://orcid.org/ 0000-0002-1864-976X

Kamal Abderrafi is a professor at Hassan II University of Casablanca, Morocco, specializing in Materials Science, Medical Physics, and Plasma Physics. With expertise in nanoparticle synthesis, nanoelectronics, and crystal engineering.
E-mail: kamal abderrafi@gmail.com
https://orcid.org/0000-0002-4349-1941

Rhma Adhiri has a 3rd cycle doctorate in solid state physics (passivation and characterization of semiconductors) in 1993 and a doctorate in materials science (manufacture and characterization of components in optoelectronics and microelectronics) in 2000 from the Hassan II University of Casablanca, Faculty of Science Ben M'sick, Morocco. She is currently a professor at the Department of Physics, the same faculty, and a head of the research team "Materials and thin layers" of the Laboratory of Engineering and Materials. Her main scientific activities fall within the field of engineering science and physics of materials: materials development by various deposition methods, development of analytical and electrical techniques, modeling and simulation.
E-mail: rahmadhiri@gmail.com, https://orcid.org/0000-0002-9595-3642

Підвищення ефективності сонячних елементів CIGS завдяки відновленому оксиду графену польового шару тильної поверхні

D. Fatihi, M.P. Bhandari, S. Golovynskyi, K. Abderrafi, R. Adhiri

Анотація. Сонячні батареї з селеніду міді, індію і галію (CIGS-SC) привернули увагу завдяки своїй економічній ефективності та екологічним характеристикам, що робить їх перспективними для майбутнього виробництва електроенергії. Ефективність CIGS-SC можна підвищити шляхом додавання польового шару тильної поверхні (BSFL) під шар поглинача для зменшення втрат на рекомбінацію. У цьому дослідженні електричні параметри, такі як послідовний опір, опір шунта та коефіцієнт ідеальності, розраховуються для CIGS-SC із передовою конструкцією за допомогою програмного забезпечення симулятора ємності сонячних батарей (SCAPS). Детальна модель, яка використовується в симуляції, враховує властивості матеріалу та процес виготовлення BSFL. З використанням відновленого оксиду графену (rGO) BSFL прогнозується ефективність перетворення на рівні 24% і значне підвищення коефіцієнта заповнення. Це підвищення, у першу чергу, пояснюється здатністю шару rGO послаблювати рекомбінацію носіїв заряду та встановлювати квазіомічний контакт на межі поділу метал-напівпровідник. При вищих температурах BSFL може стати менш ефективним через збільшення рекомбінації і, у свою чергу, зменшення тривалості життя носіїв. Загалом, це дослідження дає цінну інформацію про фізичні основи CIGS-SC з BSFL і підкреслює потенціал для підвищення їх ефективності за допомогою вдосконалених методів проектування та виготовлення.

Ключові слова: CIGS, сонячні елементи, відновлений оксид графену (rGO), польовий шар тильної поверхні, SCAPS.